LAWRENCE
LIVERMORE
NATIONAL
LABORATORY

LLNL-JRNL-537672

The Incorporation of Europium into Apatite: A New Explanation

K. Holliday, K. Dardenne, C. Walther, T. Stumpf

March 13, 2012

Radiochimica Acta

Disclaimer

Solid Solutions

DOI: 10.1002/anie.200((will be filled in by the editorial staff))

The Incorporation of Europium into Apatite: A New Explanation**

Kiel Holliday, Kathy Dardenne, Clemens Walther, and Thorsten Stumpf*

Solid solution formation is a general concept which applies to basic mineralogy,[1] health sciences,[2] nuclear waste migration,[3-6] and also to industrial scale materials doping.[7] For each of these applications a mechanistic understanding on a molecular level is required, which is, however, still lacking.[3,4] The present work applies Eu^{3+} as a spectroscopic probe to elucidate the incorporation process of trivalent actinides and lanthanides in apatite. By the use of time resolved laser fluorescence spectroscopy (TRLFS) local symmetry and number of waters in the immediate coordination sphere of the metal center is obtained even at very low concentrations (ppm and below).[3-6,8-14] Based on this data one can discriminate between incorporated and surface sorbed species.[15] Besides its unique spectroscopic properties, Eu^{3+} is also a frequently used homolog for the trivalent actinides, Pu^{3+}, Am^{3+}, and Cm^{3+} and as such a suitable tool for understanding radionuclide migration.[5] Furthermore, Eu^{3+} serves as an analogue of Gd^{3+} which is a toxic substance used in medical imaging.[8] The guest phase used in this study is apatite, because it is an important mineral for radionuclide and pollutant migration in the environment due to its ability to accommodate a large range of elements and the low solubility of actinides in phosphate media.[16,17] In addition, it is also the main component of biological hard tissue, which is the sequestration site for many heavy metal toxins within the human body.[18-20] For example, it has been observed that Pu has a greater causality for bone cancer as compared to Ra given the same activity.[21] Because of its widespread applicability over these various multidisciplinary applications, an atomic scale mechanistic understanding of the incorporation process is necessary to interpret larger scale phenomena.

[*] K. Holliday, K. Dardenne, C. Walther, T. Stumpf
Institut für Nuklear Entsorgung
Karlsruhe Institut für Technologie
P.O. Box 3640, 76021 Karlsruhe, DE
E-mail: holliday7@llnl.gov

K. Holliday
Condensed Matter and Materials Division
Lawrence Livermore National Lab
7000 East Avenue, Livermore, CA USA

C. Walther
Leibniz Universität Hannover
Institut für Radioökologie und Strahlenschutz
D-30419 Hannover, DE

[**] This work was co-financed by the Helmholtz Gemeinschaft Deutscher Forschungszentren (HGF) by supporting the Helmholtz-Hochschul-Nachwuchsgruppe "Aufklärung geochemischer Reacktionsmechanismen an der Wasser/Mineralphasen Grenzfläche". The authors thank S. Büchner for technical assistance with the laser fluorescence measurements. This work was performed under the auspices of the U.S. Department of Energy by Lawrence Livermore National Laboratory under Contract DE-AC52-07NA27344. We thank the ANKA synchrotron light source for providing the beamtime.

The doping of apatite by Eu^{3+} and other elements was previously studied, most notably by Fleet and Pan.[22] However, these studies on heat treated samples are not useful to the understanding of incorporation under environmental or biological conditions, because it has been shown that the incorporation site of Eu^{3+} is changed above 480°C.[23] The site of incorporation has been attributed to the substitution mechanism,[24] electronegativity differences,[25] bond valance,[26] and spatial accommodation,[22] but few studies have aimed at reconciling the issue of incorporation at ambient temperatures. Two notable exception are the studies by Gaft and Karbowiak.[23,27] Both studies concluded that Eu^{3+} was incorporated into the Ca(I) site of apatite, which is in obvious contradiction to the observed spectroscopic findings: the $^5D_0 \rightarrow {}^7F_1$ transition of Eu^{3+} is 3-fold split indicating a lower symmetry than C_3, which is the symmetry of the Ca(I) site. Gaft and Karbowiak explained the additional peaks from multiple site excitation, poor resolution, or contaminants due to the use of natural apatite.[23,27] The present study was designed to systematically rule out all these sources of artifacts, but still reproduces the characteristic spectra reported in previous studies.

a)

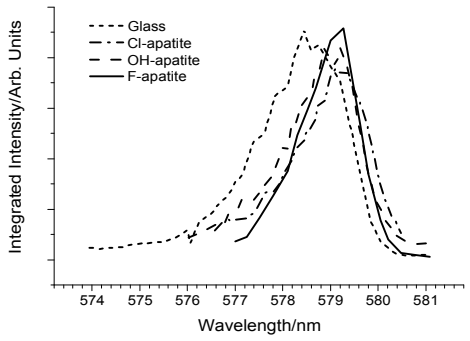

b)

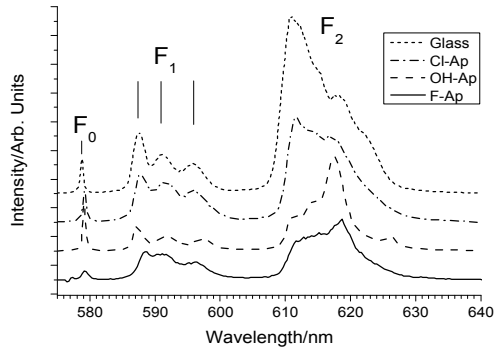

Figure 1. a) Excitation spectra and b) emission spectra from direct excitation of fluoro-, hydroxy-, and chloro-apatite as compared to calcium phosphate glass.

A satisfying explanation requires discriminating sites of different geometry, which is possible by using so called selective excitation. The laser source was tuned to the $^7F_0 \rightarrow {}^5D_0$ transition of Eu^{3+} and the fluorescence signal from the $^5D_0 \rightarrow {}^7F_i$ (i = 1-2) was integrated. Because of the single multiplicity of the transition, each Eu^{3+} species will give a unique peak.[12-14] As can be seen by Fig. 1a, this resulted in an extremely broad peak spanning several nm around a maximum at 579 nm. The broadness of the peak would suggest a continuum of Eu^{3+} environments as would be the case in an amorphous material. Further evidence of an amorphous environment can be seen when the excitation spectra are compared to that of a calcium phosphate glass (Fig. 1a).

The emission spectra were recorded after direct excitation to the $^5D_0$ state (Fig. 1b). Clearly, there is a 3-fold splitting of the $^5D_0 \rightarrow {}^7F_1$ transition indicating that the symmetry is lower than the C_3 symmetry of the Ca(I) site in apatite (Fig. 1b labelled F_1). The emission spectra compare well with that of the amorphous glass sample suggesting a similar local environment. It should be noted that the excitation energy and emission spectra are consistent with previous studies.[23,27]

X-ray absorption fine structure (XAFS) spectroscopy was performed on chloro-apatite as a complimentary technique to TRLFS. Results from the fit are shown in Table 1 as compared to the Ca(I) site of chloro-apatite.[28] The data with fit can be found in supplemental information. The nearest neighbor oxygen were fit with a single distance in the experimental data, because it was found that adding an additional oxygen distance did not improve the fit. In apatite the oxygen atoms around the Ca(I) site appear at two distinct distances, so the distance from Ca(I) to first shell oxygen atoms are reported as a weighted average for comparison. As can be seen from Table 1, the first shell of oxygen atoms are 0.22 Å closer than expected for the Ca(I) site. This would be consistent with a contraction due to the less restrained amorphous local environment and is what would be expected from bond valence theory. This effect is less pronounced in the phosphorous shell, which is 0.12 Å closer than would be expected. There is also intensity that can only be fit with a chlorine atom at 2.74 Å. The only explanation for this is that Eu^{3+} is not substituted on the Ca(I) site, because there is no chlorine atom in the local environment of the Ca(I) site. The Eu^{3+} is also not substituted on the Ca(II) site, because it can be driven there by heating producing a completely different fluorescence behaviour.

Table 1. Fitted XAFS parameters as compared to the expected values from substitution on a Ca(I) site.[27]

Bond	R (Å)	N	σ^2 (Å^2)	E_0 (eV)
Eu – O	2.32	4.4	0.002	3.7
Ca(I) – O	2.54	9	-	-
Eu – P	3.08	3.3	0.002	3.7
Ca(I) – p	3.20	3	-	-
Eu – Cl	2.74	2	0.0006	3.7
Ca(I) – Cl	5.50	-	-	-

A sample of the hydroxy-apatite was heated to 800°C for 4 hours. The excitation spectra on the resulting sample show a dominant peak at 574.0 nm indicating the formation of a new species and two minor species at 579.4 and 577.7 nm (Fig. 2a). These two minor species are in the same wavelengths as the broad range of species found before heat treatment, and are therefore assumed to be similar to the Eu^{3+} environment before heat treatment (Fig. 2a). The new dominant species at 574.0 nm is consistent with previous studies which have identified it as Eu^{3+} occupying the Ca(II) site in apatite.[23]

The emission spectra from direct excitation of each species can be seen in Fig. 2b. It was found that by exciting the $^7F_0 \rightarrow {}^5D_0$ transition of the low energy species at 579.4 nm, there was sufficient overlap with the $^7F_1 \rightarrow {}^5D_0$ band of the more abundant high energy species (574.0 nm) to contribute peaks to the emission spectra.

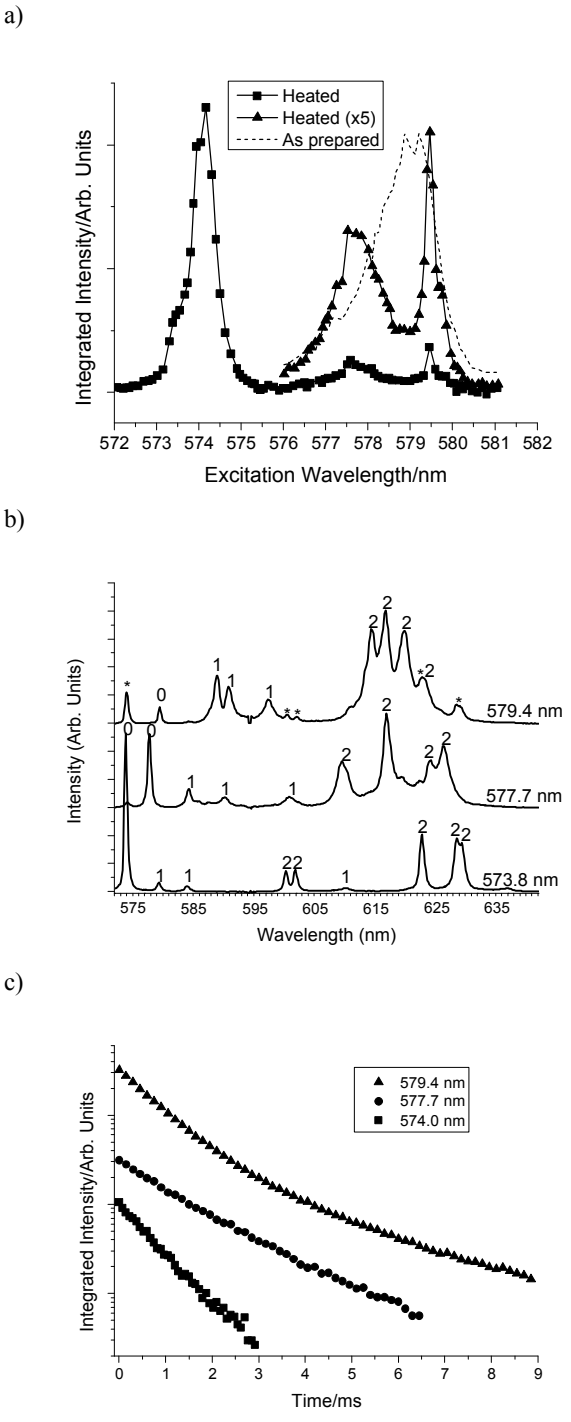

Figure 2. a) Excitation spectra b) emission spectra from direct excitation and c) fluorescence lifetimes of hydroxy-apatite after heat treatment. Excitation wavelength indicated in b) and c). * indicate peak from interfering species and number indicates ΔJ in b).

These peaks are marked with (*) and can be ignored as they are a contribution from an interfering species (Fig. 2b). The two lower energy species excited at 579.4 and 577.7 nm give an indication of the Eu^{3+} environment before heat treatment since they are excited in the same energy range. These spectra show further evidence that Eu^{3+} does not occupy the Ca(I) site. Both these species have a 3-fold splitting of the $^5D_0 \rightarrow {}^7F_1$ transition (labelled with 1 in Fig. 2b) and a 4-fold splitting of the $^5D_0 \rightarrow {}^7F_2$ transition (labelled with 2 in Fig. 2b) indicating a C_{2V} symmetry. This would not be possible in either cation site of the apatite lattice. The new dominant species excited at 574.0 nm has such an extreme splitting of these two transitions that they overlap and show the maximum 3-fold and 5-fold splitting for the $^5D_0 \rightarrow {}^7F_{1,2}$ transitions. This has been shown to be consistent with the spectrum expected for Eu^{3+} occupying the Ca(II) in apatite.[29] Given the hypothesis that the Eu^{3+} is located in grain boundaries before heat treatment, this can now be explained by a crystallization process from grain growth at elevated temperatures. This would be more likely than the previous explanation of ion diffusion from Ca(I) to Ca(II) in apatite at 480°C.[22] Recently, it has been shown that the most probable diffusion pathways for Ca^{2+} in apatite does not result in an exchange of Ca(I) and Ca(II).[30]

Finally, the number of coordinating water molecules is measured for each site. The fluorescence decay after selective excitation is observed time resolved for each species (Fig. 2c). The high energy species at 574.0 nm was found to have a mono-exponential lifetime of 0.8 ms (Fig. 2c). This has been attributed to the charge compensation mechanism replacing X^- (F^-, Cl^-, or OH^-) with O^{2-} and forming a covalent Eu-O bond.[23,27,31] While a Eu-O covalent bond may exist, it should be pointed out that the charge compensation would have occurred before the sample was heated. The lowest energy species (579.4 nm) has a bi-exponential lifetime with a fast component of 0.7 ms confirming the interference from the dominant species found at 574.0 nm (Fig. 2c). The long component from the 579.4 nm species has a lifetime of 2.8 ms. The species with excitation energy of 577.7 nm has a lifetime of 1.0 ms (Fig. 2c). This supports previous studies which suggested that the species at 577.7 nm is an intermediate species.[23] This is more acceptable as a crystallization process through grain growth than an intermediate found in a diffusion process from the Ca(I) site to the Ca(II) site in apatite, because there would be no site readily available within the diffusion process.[30]

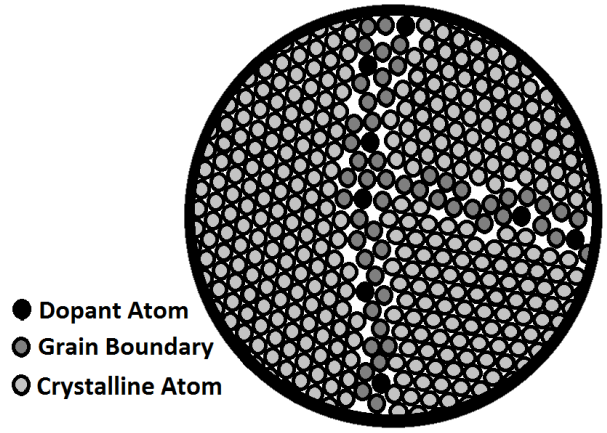

Figure 3. Graphical representation of the incorporation of Eu^{3+} into the grain boundaries of apatite.

Concluding, this study provides clear evidence that at ambient temperatures relevant to biological and environmental processes Eu^{3+} does not incorporate into the Ca(I) site through isomorphic substitution as previously presumed. Instead, it accumulates into amorphous grain boundaries adopting a different local symmetry than both Ca(I and II) sites within the apatite structure. A simplified cartoon of this concept is presented in Fig. 3. Upon heating the sample the Eu^{3+} is incorporated into the Ca(II) site. This is likely a result of a crystallization process from grain growth as opposed to ion diffusion. This new insight has an impact on fundamental mineralogy, radionuclide and pollutant migration, and the incorporation of heavy metals into biological hard tissue. Revisiting the example from the introduction, the greater radiotoxicity of Pu as compared to Ra can be attributed to the high local concentration within grain boundaries greatly increasing the local dose in small areas, i.e. for single neighboring cells. The results from this study will also increase the fundamental understanding of the incorporation process into other complex phases.

Experimental Section

Apatite was synthesized by coprecipitation of calcium and phosphate at basic pH. Solutions were mixed in the 5:3 calcium to phosphate ratio and brought to pH 11 with sodium hydroxide. The solid was recovered by filtration and subsequently heated to 700°C to improve crystallinity. The powder XRD patterns were collected on a Bruker D8 diffractometer. Phases were identified using Bruker-AXS EVA software. Batch studies were performed by placing the solution containing the doping ion in contact with apatite for up to 100 days, while controlling ionic strength, solid to liquid ratio, pH, and doping ion concentration. Flow-through-cell experiments control similar parameters; however, cation, anion and doping solutions are fed into a chamber that contains seed crystals of apatite with mixing. A calcium phosphate glass was made by quickly cooling a calcium phosphate mixture from the melt. TRLFS was performed using a XeCl-eximer laser pumped dye laser. The detection system was calibrated using a neon lamp and the laser wavelength was monitored. Fluorescence measurements were detected by an optical multichannel analyzer that consists of a polychrometer with 300/600/1200 lines/mm gratings and an intensified, gated photodiode array. The samples were cooled to 4 K by a helium refigerated cryostat to improve resolution. EXAFS spectra were recorded at the INE-beamline at ANKA (Germany). EXAFS data analysis was performed using standard procedures in Athena and Artemis interfaces of the iFEFFIT software. The overall scaling factor S_0^2 was held constant at 0.85 after its determination on a standard sample. Distances are determined with an error of 0.02 Å and coordination numbers with an error of 20%. Further detail on the methods can be found in supplemental information.

Received: ((will be filled in by the editorial staff))
Published online on ((will be filled in by the editorial staff))

Keywords: Fluorescence spectroscopy · EXAFS spectroscopy · Apatite · Rare Earths · Incorporation

[1] S. Sauve, W. Hendershot, H.E. Allen, *Environ. Sci. Tech.* **2000**, *34*, 1125-1131; J.A. Davis, C.C. Fuller, A.D. Cook, *Geochim. Cosmochim. Acta* **1987**, *51*, 1477-1490; R.G. Berman, L.Y. Aranovich, *Contrib. Mineral. Petr.* **1996**, *126*, 1-24.

[2] K.A. Gross, L.M. Rodriguez-Lorenzo, *Biomater.* **2004**, *25*, 1375-1384.

[3] M. Schmidt, T. Stumpf, C. Walther, H. Geckeis, T. Fanghänel, *Dalton Trans.* **2009**, *33*, 6645-6650.

[4] M. Schmidt, T. Stumpf, M.M. Fernandes, C. Walther, T. Fanghänel, *Angew. Chem. Int. Ed.* **2008**, *47*, 5846-5850.

[5] R.J. Silva, H. Nitsche, *Radiochim. Acta*, **1995**, *70/71*, 377-396.
[6] K. Holliday, A. Chagneau, M. Schmidt, F. Claret, T. Schäfer, T. Stumpf, *Dalton Trans.* **2012**, DOI: 10.1039/c2dt12425d.
[7] M.S. Islam, D.J. Driscoll, C.A.J. Fisher, P.R. Slater, *Chem. Mater.* **2005**, *17*, 5085-5092; Y. Iwahashi, Z. Horita, M. Nemoto, T.G. Langdon, *Metall. Mater. Trans. A* **1998**, *29A*, 2503-2510.
[8] J.-C.G. Bünzli, H.G. Brittain, G.W. DeVore, W. Loveland in *Lanthanide Probes in Life, Chemical and Earth Sciences*, (Eds: J.-C.G. Bünzli, G.R. Choppin) ELSEVIER, Amsterdam, **1989**, 219-408.
[9] G. Geipel, *Coord. Chem. Rev.* **2006**, *250*, 844-854.
[10] J.-C.G. Bünzli, G. Piguet, *Chem. Soc. Rev.* **2005**, *34*, 1048-1077.
[11] I. Hemmilä, V. Laitala, *J. Fluoresc.* **2005**, *15*, 529-542.
[12] G.R. Choppin, D.R. Peterman, *Coord. Chem. Rev.* **1998**, *174*, 283-299.
[13] B.R. Judd, *Phys. Rev.* **1962**, *127*, 750-761.
[14] D.J. Newman, *Adv. Phys.* **1971**, *20*, 197-256.
[15] W.DeW. Horrocks, Jr., D.R. Sudnick, *J. Am. Chem. Soc.* **1979**, *101*, 334-340.
[16] S. Handley-Sidhu, J.C. Renshaw, P. Yong, R. Kerley, L.E. Macaskie, *Biotechnol. Lett.* **2011**, *33*, 79-87.
[17] F.G. Simon, V. Biermann, C. Segebade, M. Hedrich, *Sci. Total Environ.* **2004**, *326*, 249-256.
[18] E. Polig, F.W. Bruenger, R.D. Lloyd, S.C. Miller, *Health Phys.* **1998**, *75*, 251-258.
[19] M.D. Wood, N.A. Beresford, D.V. Semenov, T.L. Yankovich, D. Copplestone, *Radiat. Environ. Biophys.* **2010**, *49*, 509-530.
[20] R.A. Guilmette, G.M. Kanapilly, D.L. Lundgren, A.F. Eidson, *Health Phys.* **1984**, *46*, 845-858.
[21] N.D. Priest, S. Jackson, *Int. J. Radiat. Biol.* **1977**, *32*, 325-350.
[22] M.E. Fleet, Y. Pan, *J. Solid State Chem.* **1994**, *112*, 78-81; M.E. Fleet, Y. Pan, *Amer. Mineral.* **1995**, *80*, 329-335; M.E. Fleet, Y. Pan, *Geochim. Cosmochim. Acta* **1997**, *61*, 4745-4760; M.E. Fleet, X. Liu, Y. Pan, *Amer. Mineral.* **2000**, *85*, 1437-1446.
[23] M. Karbowiak, S. Hubert, *J. Alloy Compd.* **2000**, *302*, 87-93.
[24] P.E. Mackie, R.A. Young, *J. Appl. Crystallogr.* **1973**, *6*, 26-31.
[25] V.S. Urusov, V.O. Khudolozhkin, *Geochem. Int.* **1975**, *11*, 1048-1053.
[26] J.M. Hughes, M. Cameron, A.N. Mariano, *Amer. Mineral.* **1991**, *76*, 1165-1173.
[27] M. Gaft, L. Nagli, R. Reisfeld, G. Panczer, M. Brestel, *J. Lumin.* **1997**, *72-74*, 572-574.
[28] T.J. White, D. ZhiLi, *Acta Cryst.* **2003**, *B59*, 1-16.
[29] K. Voronko, G. Maksimova, A. Sobol, *Opt. Spectrosc. (USSR)* **1991**, *70*, 203-206.
[30] E.E. Jay, P.M. Mallinson, S.K. Fong, B.L. Metcalfe, R.W. Grimes, *J. Mater. Sci.* **2011**, *46*, 7459-7465.
[31] F.M. Ryan, R.W. Warren, R.H. Hopkins, J. Murphy, *J. Electrochem. Soc. Solid State Sci.* **1978**, *125*, 1493-1498.

Entry for the Table of Contents

Layout 1:

Solid Solutions

Kiel Holliday*, Kathy Dardenne, Clemens Walther, and Thorsten Stumpf

_____ **Page – Page**

The Incorporation of Europium into Apatite: A New Explanation

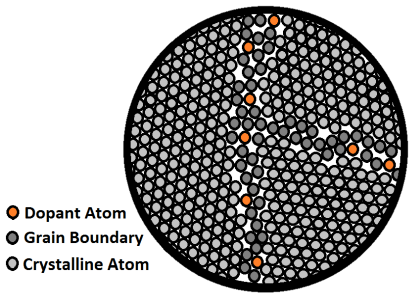

Not isomorphic substitution: Although europium incorporates into apatite under environmental and biological conditions, it was shown by TRLFS and EXAFS that it does not substitute for a cation site within the crystal structure. Instead the europium occupies positions within the grain boundaries of the polycrystalline apatite. These findings have implications for radionuclide migration and incorporation into biological hard tissue.

Supplemental Information

Full Methods

Apatite synthesis

All chemicals were reagent grade and purchased from Alpha Aesar. Concentrated solutions of calcium chloride and sodium hydrogen phosphate were made by dissolving in 18 MΩ/cm water. These solutions were then mixed in the 5:3 calcium to phosphate ratio and brought to pH 11 with sodium hydroxide for hydroxy-apatite or allowed to remain at natural pH and NaF or NaCl was added in order to produce fluoro- or chloro-apatite respectively. The solution was stirred for 24 hours before the solid was collected via filtration. This solid was dried and subsequently heated to 700°C to improve crystallinity.

X-ray diffraction (XRD)

Samples were ground to a fine powder and spread in a thin layer over a low-background sample holder (single crystal silicon wafer) with the aid of methanol. The powder XRD patterns were collected on a Bruker D8 Advance diffractometer, using a Cu anode (wavelength $K\alpha_1$ at 0.1540598 nm). Patterns were taken using an acceleration of 40 mV and current of 40 mA over a range from 10 to 120 $^{o}2\theta$ with a step size of 0.01 $^{o}2\theta$ and 4 seconds per step. Phases were identified using Bruker-AXS EVA software.

Batch studies

Batch studies were performed simply by placing the solution containing the doping ion in contact with hydroxy-apatite, while controlling ionic strength, solid to liquid ratio, pH, and doping ion concentration. The solution containing the doping ion was 10.0 mM sodium perchlorate to maintain ionic strength and was adjusted to pH of 6 with sodium hydroxide and perchloric acid as needed before being added to the apatite at a solid to liquid ratio of 2.0 g/L. The Eu^{3+} concentration was 1.0 μM. Samples were occasionally stirred over the contact time of 100 days.

Flow-through-cell studies

Three solutions are used to feed a chamber containing approximately 150 mg of the parent mineral apatite, which is stirred at 850 rot min^{-1}. These three feed solutions are pumped into the chamber at 0.1 mL min^{-1} each and contain the cation, anion, and doping solution, respectively. Each solution is prepared with 10.0 mM $NaClO_4$ as a background electrolyte to maintain ionic strength. By maintaining a low saturation index (SI), surface growth controlled precipitation is the dominant process. All chemicals are reagent grade purchased from Alpha Aesar. Further details can be found in a previous publication.[3]

Time resolved laser fluorescence spectroscopy (TRLFS)

TRLFS was performed using a pulsed (20 Hz) XeCl-eximer laser (Lambda Physics, EMG, 308 nm) pumped dye laser (Lambda Scanmate). The laser dye QUI was used for UV excitation at 394.0 nm, and Rhodamine 6G for direct excitation of Eu in the range from 573 – 582 nm. The laser wavelength was monitored using a Toptica WS7 wavemeter (>10^{-5} nm accuracy). Fluorescence measurements were detected by an optical multichannel analyzer that consists of a polychrometer with

300/600/1200 lines/mm gratings (Jobin Yvon) and an intensified, gated photodiode array (Spectroscopy Instruments). Maximum resolution at 300 and 1200 lines/mm was measured to be 0.9 and 0.2 nm, respectively. The detection system was calibrated with a neon lamp (Pen Ray 6032). The samples were cooled to 4 K by a helium refrigerated cryostat (CTI-cryogenics) to improve resolution. For the discrimination of Rayleigh and Raman scattering the minimum gate delay between laser pulse and camera gating was set to 1.0 µs. The gate width of the camera was fixed at 10 ms to ensure the collection of the entire fluorescence signal. Fluorescence lifetime measurements were made with a delay time step between 50 and 150 µs and a total of 60 steps were taken for each lifetime measurement.

Extended x-ray absorption fine structure (EXAFS)

Europium L3-edge and L2-edge spectra were recorded at the INE-beamline at ANKA (Germany) using a double-crystal monochromator equipped with a pair of Si(111) crystals. The DCM is operated in fixed-exit mode. The incident intensity is held constant by means of a piezo-driven feedback system. The parallel alignment of the crystal faces is detuned to ~70% of the maximum beam intensity. The samples powders were mounted in Kapton tape. Measurements were made in fluorescence mode using a five elements LEGe detector (Canberra) with a sample orientation of 45° to the incident beam. The energy calibration was performed using a Fe metal foil (K edge at 7112 eV). EXAFS data analysis was performed using standard procedures in Athena and Artemis interfaces[32] of the iFEFFIT software.[33] The overall scaling factor S_0^2 was held constant at 0.85 after its determination on a standard sample. Distances are determined with an error of 0.02 Å and coordination numbers with an error of 20%.

[3] Schmidt, M., Stumpf, T., Walther, C., Geckeis, H., Fanghänel, T., *Dalton Trans.*, 2009, **33**, 6645.

[32] Ravel, B., Newville, M. *J. Synchrotron Rad.* **2005,** *12,* 537.

[33] Newville, M. *J. Synchrotron Rad.* **2001,** *8,* 322.

Supplemental Figure 1

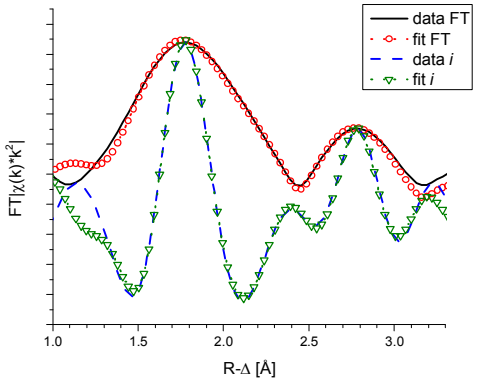

a)

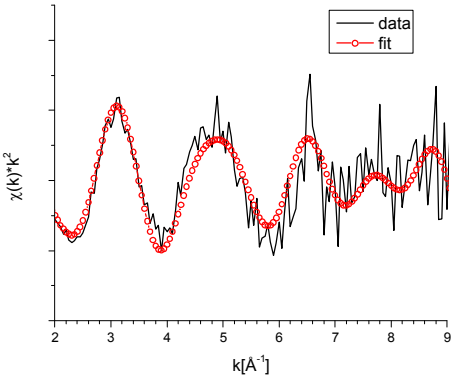

b)

Supplemental Figure 1: EXAFS data with fit of Eu^{3+} doped chloro-apatite a) FT magnitude (thick solid line), imaginary part (dashed line), and fit results (open triangles and circles). FT is performed in the range 1.290-3.185 Å. b) k^2-weighted Eu^{3+} L3 EXAFS of the sample (solid line) and fit result (open circles). Data was fit in the range 2.179-8.969 $Å^{-1}$. The residual of the fit was 1.1 %.